Journal of Applied Polymer Science

Copper (I) ion stabilized on Fe_3O_4-core ethylated branched polyethyleneimine-shell as magnetically recyclable catalyst for ATRP reaction

Mohammad Reza Nabid, Yasamin Bide, Nastaran Ghalavand
Faculty of Chemistry, Department of Polymer, Shahid Beheshti University, G.C., P.O. Box 1983969411 Tehran, Iran
Correspondence to: M. R. Nabid (E-mail: m-nabid@sbu.ac.ir)

ABSTRACT: Branched polyethyleneimine (bPEI) was used to modify the surface of Fe_3O_4 nanoparticles coated with silica layer, and then, it was treated with ethyl iodide to prepare Fe_3O_4@SiO_2@Ethylated-bPEI. In the next step, the yolk–shell structure was gained by selectively etching the SiO_2 middle layer. Finally, copper(I) was introduced to the yolk–shell Fe_3O_4@Ethylated-bPEI and the activity of the catalyst was evaluated for atom transfer radical polymerization (ATRP) of styrene, led to obtain the well-defined polymer with relatively low polydispersity. The toxicity of the residual copper in the polymer product was a limiting issue for applicability of ATRP reactions especially for biological purposes. In this report, the copper content in the polymer was reduced to the excellent value of 1.1 ppm. Moreover, the magnetic isolation, recyclability, and remove the need for an external ligand were other advantages of the synthesized catalyst which makes it suitable for employing in ATRP reactions. © 2015 Wiley Periodicals, Inc. J. Appl. Polym. Sci. **2015**, *132*, 42337.

KEYWORDS: ATRP reaction; branched polymer; catalysts; magnetic nanoparticles; yolk-shell

Received 4 March 2015; accepted 8 April 2015
DOI: 10.1002/app.42337

INTRODUCTION

Atom transfer radical polymerization (ATRP) a living polymerization technique, has been attracted significant interest in the recent years.[1] ATRP is a robust and powerful tool that permits the synthesis of well defined and advanced polymeric materials with predetermined molecular weights, relatively low disparities, and high degrees of chain end functionalities.[2,3] In general, the ATRP technique consists of an alkyl halide initiator, a transition metal ion which can exist in two different oxidation states,[4] and a ligand with ability to form a complex with the metal ion.[5,6] A wide variety of transition metals have been used as ATRP catalyst including Ni, Re, Ti, Os, Cu, Co, etc.,[6–11] which copper is the most common.[11–13]

A limitation of the ATRP technique is the need to use high concentration of transition metal catalyst for keeping a favorable redox equilibrium, which may cause the post-purification of the polymer from the catalyst contamination.[14] A key technical hurdle associated for industrial application of ATRP is the effective removal of the copper catalyst from the polymer.[15] Several procedures for the catalyst removal have been developed, that is, extraction, precipitation, treatment with MeOH, Na_2S, and biphasic systems, however these techniques have disadvantages such as their cost, loss of polymer, and difficulties in separating catalyst from polymerization mixture.[12,16–19] A potential solution for this problem is the immobilization of the catalyst on the solid support which provide a more effective way for separating, and recycling the catalyst. Mostly, these materials are based on the Cu(I) complexes with nitrogen containing ligands because of their high efficiency and less cost.[20,21] The essential factor which should be considered is the electronic interactions of nitrogen-based ligand with the Cu center. Polyethyleneimine (PEI) is a hydrophilic polymer with varying molecular weight, topology and shape.[22] In 2011, Zorvaryan and coworkers synthesized alkylated linear polyethyleneimine ligands for ATRP reaction of styrene and methyl methacrylate. They found that the homogeneous polymerization in a controlled fashion and relatively fast reactions compared with other ATRP ligands were performed.[23]

Linear PEI contains all secondary amines, while branched PEI has high-density of amine groups consisting of primary, secondary and tertiary amino group. So, branched PEI is a unique choice as a polymeric support for copper ions in ATRP reactions, because of their important advantages such as exact functionality, being readily available in various molecular weights and also being cheaper than other branched polymers.[24,25]

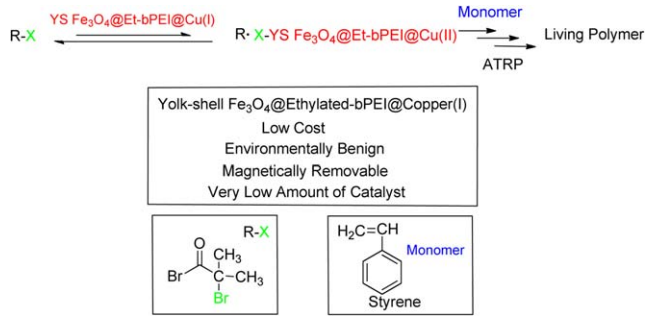

Scheme 1. Living radical polymerization of styrene with Cu(I)@YS Fe_3O_4@Et-bPEI. [Color figure can be viewed in the online issue, which is available at wileyonlinelibrary.com.]

Yolk–shell structure is a special class of core-shell structure with a core@void@shell configuration.[26,27] The yolk–shell structures which possess a movable core inside a hollow capsule have received extensive attention due to their unique properties and increasing and important applications in catalysis, controlled released, and lithium-ion batteries.[28–33] Compared with core-shell composites, hollow structures have higher surface area, lower density, and larger vacant space.[29,34] Among these structure, the yolk–shell composites with a movable magnetic core and a functional shell are a good choice as catalyst supports because of their easy extraction from the reaction mixture and removing the need for filtration or centrifugation.[35,36]

Following our interesting in the development of sustainable benign pathways for organic transformations, and nano-catalysis,[37–43] herien, we described a facile and efficient strategy for synthesis of yolk–shell structure with Fe_3O_4 core and alkylated polyethyleneimine shell as a support for stabilizing copper(I) (Cu(I)@YS Fe_3O_4@Et-bPEI) as a recylable catalyst for ATRP reaction of styrene (Scheme 1).

EXPERIMENTAL

Materials

Ferric chloride hexahydrate ($FeCl_3 \cdot 6H_2O$), trisodium citrate dehydrate, sodium acetate (NaAc), ethylene glycol (EG), ethyl iodide, 2-bormo isobutyryl bromide (BIBB), and tetraethyl orthosilicate (TEOS) were purchased from Merck Chem. Co. Branched polyethyleneimine (bPEI) solution 50% (w/v) in H_2O ($M_w = 7{,}50{,}000$ g/mol) was supplied from Fluka. Copper(I) bromide (CuBr, 98%) was purchased from Aldrich Chemical Co. Styrene was distilled over calcium hydride under reduced pressure before polymerization. All other chemicals were purchased from Aldrich or Merck companies and used as received without any further purification.

Synthesis

Synthesis of Fe_3O_4 Nanoparticles. The magnetic Fe_3O_4 nanoparticles were prepared through a solvothermal reaction.[44] Briefly, $FeCl_3 \cdot 6H_2O$ (3.24 g, 12 mmol), trisodium citrate (0.6 g, 2.3 mmol), and sodium acetate (3.6 g, 43.9 mmol) were dissolved in ethylene glycol (60 mL) under vigorous stirring at room temperature. After stirring about 30 min, the mixture was transferred into a 100 mL Teflon stainless-steel autoclave and was heated at 200°C for 10 h to yield a homogeneous yellow solution. Then, the autoclave was allowed to cool to room temperature. The obtained Fe_3O_4 particle suspension was washed successively with H_2O and EtOH three times and then dried in a vacuum oven for 12 h at room temperature.

Preparation of Fe_3O_4@SiO_2 Particles. About 50 mL of as-prepared Fe_3O_4 nanoparticles solution (containing 0.4 g Fe_3O_4) was dispersed into the mixture of deionized water (10 mL), ethanol (100 mL), and $NH_3 \cdot H_2O$ (50 mL). After imposing to ultrasonic radiation for 10 min, a certain amount of TEOS was quickly added into the system. The reaction was allowed to proceed with stirring for 8 h at room temperature. Finally, the product was separated with magnet and washed with deionized water for the next-step.

Preparation of Fe_3O_4@SiO_2@bPEI. The bPEI was dispersed in ethanol (10 mg/ml), and then, an equal amount of Fe_3O_4@SiO_2 was added into the 1 mL of the above solution under sonication, and the reaction was allowed to proceed at room temperature for 24 h under stirring. After the reaction, the resultant

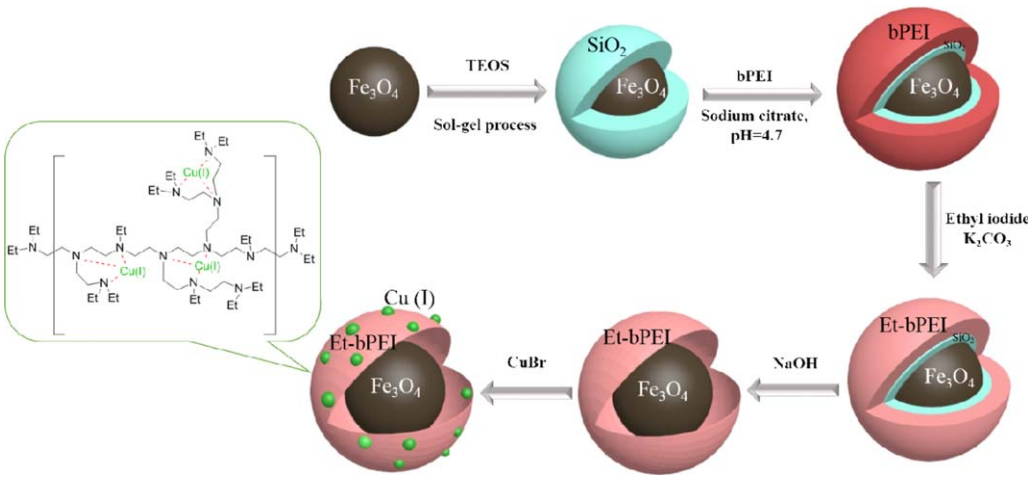

Scheme 2. The diagram of the synthesis of YS Fe_3O_4@Et-bPEI@Cu(I). [Color figure can be viewed in the online issue, which is available at wileyonlinelibrary.com.]

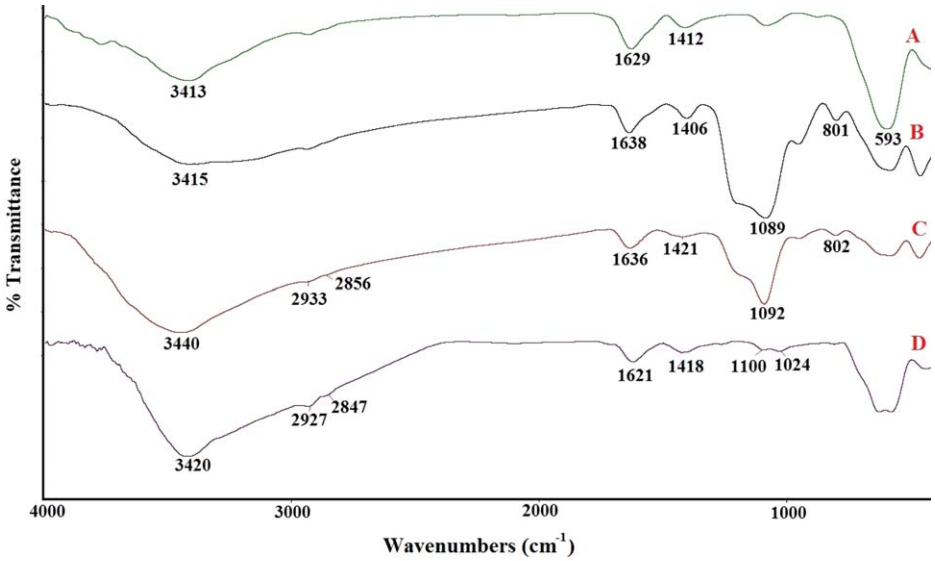

Figure 1. FT-IR spectra of the as-prepared Fe_3O_4 (**A**), Fe_3O_4@SiO_2 (**B**), Fe_3O_4@SiO_2@bPEI (**C**), and YS Fe_3O_4@Et-bPEI (**D**). [Color figure can be viewed in the online issue, which is available at wileyonlinelibrary.com.]

product was magnetically separated, washed with H_2O and EtOH three times and dried for 24 h in vacuum oven at 50°C.

Synthesis of Fe_3O_4@SiO_2@Ethylated-bPEI. Iodoethane (6 mL, 75 mmol) was placed into a 250 mL round-bottom flask with 30 mL ethanol. While the solution was stirred at room temperature, Fe_3O_4@SiO_2@bPEI (0.6 g) and potassium carbonate (1.9 g, 13.7 mmol) were added to the solution, and the mixture was refluxed for 3 days. After addition of a second amount of potassium carbonate (1.9 g, 13.7 mmol), the reaction mixture was refluxed for three more days. Subsequently, the precipitate was separated by magnetic separator, washed three times with deionized water and ethanol, and dried for 24 h in vacuum oven at 60°C.

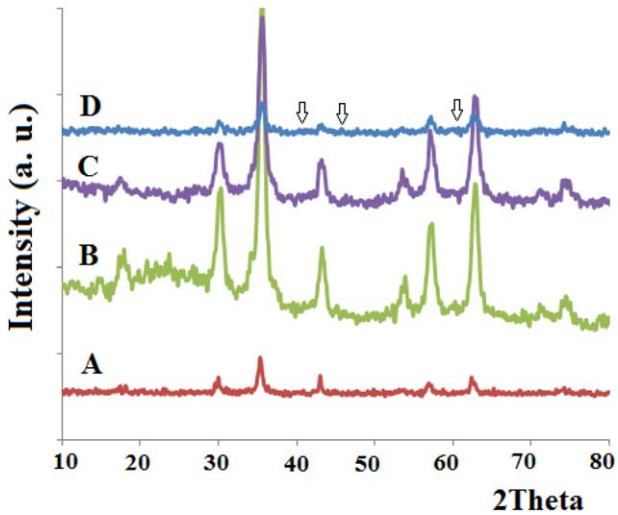

Figure 2. XRD patterns of Fe_3O_4 (**A**), Fe_3O_4@SiO_2@bPEI (**B**), YS Fe_3O_4@Et-bPEI (**C**), and YS Fe_3O_4@Et-bPEI@Cu(I) (**D**). [Color figure can be viewed in the online issue, which is available at wileyonlinelibrary.com.]

Preparation of Yolk–Shell Fe_3O_4@Ethylated-bPEI. The synthesized Fe_3O_4@SiO_2@Ethylated-bPEI composite was soaked in 1.0*M* NaOH solution under mechanical stirring for 12 h and the SiO_2 layer between the Et-bPEI shell and the Fe_3O_4 core was selectively etched. The black product was washed with deionized water and ethanol several times and dried in oven.

Preparation of Yolk–Shell Fe_3O_4@Ethylated-bPEI@Copper(I). About 0.02 g CuBr was dissolved in a minimum of dry acetonitrile. It was transferred into a 50 mL around-bottom flask containing 0.01 g of yolk–shell Fe_3O_4@Et-bPEI composite and the mixture was refluxed for 23 h. The solid product was magnetically separated, washed with dry acetonitrile, and dried in oven. The amount of Cu stabilized on the yolk–shell structure was estimated with atomic absorption spectroscopy (AAS) to be 3.8% (w/w).

General Procedure for the ATRP Reaction of Styrene. About 0.01 g YS Fe_3O_4@Et-bPEI@Cu(I) was added to a Schlenk flask equipped with a stir bar, which was previously flamed, under

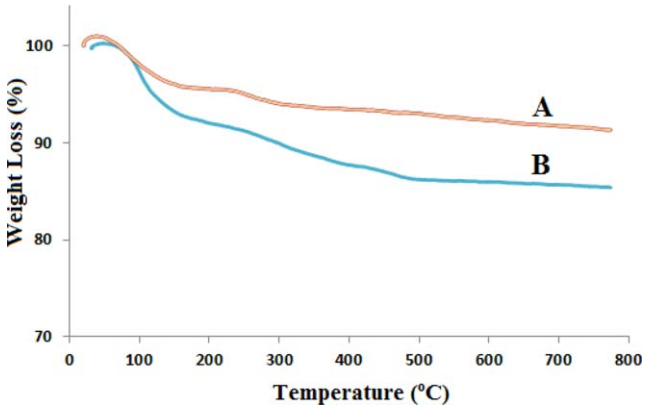

Figure 3. TGA curves of Fe_3O_4@SiO_2 (**A**) and Fe_3O_4@SiO_2@Et-bPEI (**B**). [Color figure can be viewed in the online issue, which is available at wileyonlinelibrary.com.]

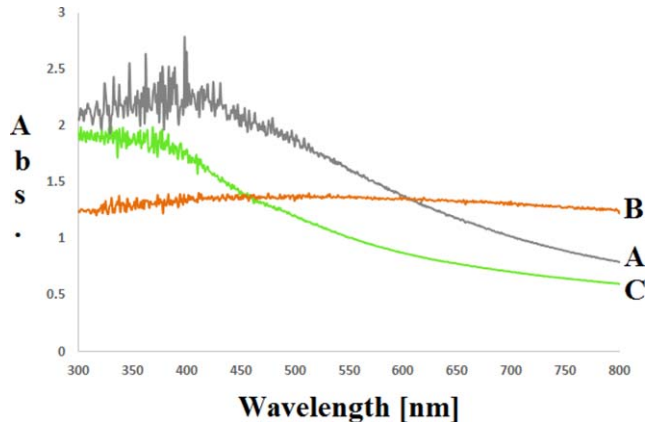

Figure 4. UV–vis spectra of Fe_3O_4@SiO_2@Et-bPEI, YS Fe_3O_4@Et-bPEI, and YS Fe_3O_4@Et-bPEI@Cu(I) in acetonitrile. [Color figure can be viewed in the online issue, which is available at wileyonlinelibrary.com.]

vacuum, cooled, and flushed with nitrogen. After it was sealed with a rubber septum, the flask was degassed and backfilled with nitrogen three times, and then was left under nitrogen. About 3 mL of toluene was deoxygenated and introduced via a syringe. Subsequently, 1 mL styrene (3.95 mmol), and anisole (0.1 mL) as a gas chromatography standard were added. The mixture was then frozen with liquid nitrogen, and three thaw–freeze cycles were performed to remove the residual oxygen from the system. The initiator 4.85 μL BIBB (0.0395 mmol) was introduced with a syringe, and the vial was placed in an oil bath and stirred at 90°C. Then, the catalyst was removed via an external magnetic field, and the polymer was precipitated in 10 mL of cool methanol, filtered, and dried as light yellow powders. For calculating the conversions at different times by gas chromatography, 1 mL of sample was removed via a syringe and after the magnetically removal of the catalyst, it was placed in a vial containing 1.5 mL tetrahydrofuran in dry-ice bath which gave 21%, 28%, 35% conversions after 1.5, 2.5, and 4.5 h, respectively.

Characterization

IR spectra were recorded on a Bomem MB-Series FT-IR spectrophotometer. Transmission electron microscopy (TEM) analyses were performed by LEO 912AB electron microscope. Ultrasonic bath (EUROSONIC® 4D ultrasound cleaner with a frequency of 50 kHz and an output power of 350 W) was used to disperse materials in solvents. Thermogravimetric analysis (TGA) was carried out using STA 1500 instrument at a heating rate of 10°C/min in air. X-ray powder diffraction (XRD) data were collected on an XD-3A diffractometer using Cu $K\alpha$ radiation. UV–vis spectra were obtained using a Shimadzu UV-2100 spectrophotometer. ^{1}H NMR spectra were recorded with a BRUKER DRX-300 AVANCE spectrometer, and DMSO or $CDCl_3$ were used as solvents. Scanning electron microscopy (SEM) was performed on a Zeiss Supra 55 VP SEM instrument. The monomer conversions were determined from the concentration of the residual monomer measured by gas chromatography using a Varian 3900 gas chromatograph (GC). Gel permeation chromatography (GPC) was performed by using GPC Agilent 1100 model and Agilent and PL gel 3 μm 300 × 7.5 mm column. AA-680 Shimadzu (Kyoto, Japan) flame atomic absorption spectrometer (AAS) with a deuterium background corrector was used for determination of the copper. The magnetization of the samples in a variable magnetic field was

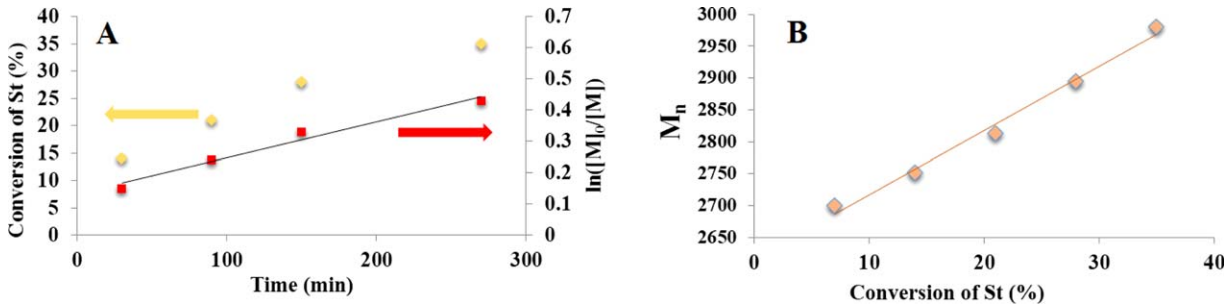

Figure 5. SEM and TEM images of YS Fe_3O_4@Et-bPEI@Cu(I).

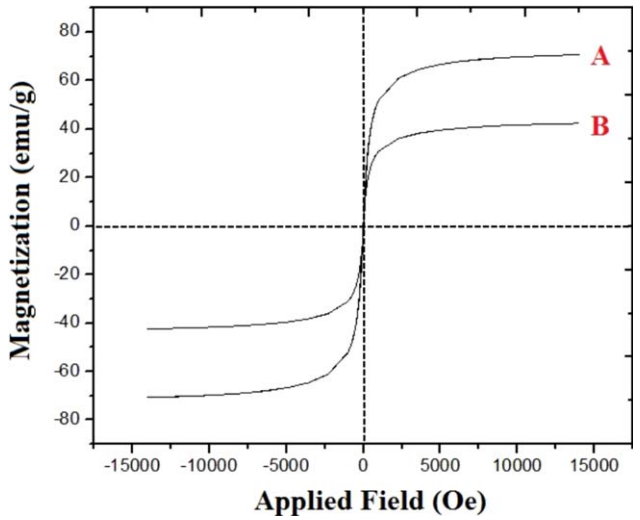

Figure 6. VSM curves of Fe_3O_4 (**A**), and YS Fe_3O_4@Et-bPEI@Cu(I) (**B**). [Color figure can be viewed in the online issue, which is available at wileyonlinelibrary.com.]

measured using a vibrating sample magnetometer (VSM) with a sensitivity of 10^{-3} EMU and a magnetic field of up to 8 kOe. The magnetic field was changed uniformly at a rate of 66 Oe/s.

RESULTS AND DISCUSSION

Synthesis of the Catalyst

Scheme 2 illustrates the practical procedure for the synthesis of YS Fe_3O_4@Et-bPEI@Cu(I) including six steps. First, the magnetite particles were synthesized through a solvothermal method at 200°C according to the literature by Liu *et al.*[44] In this reaction, $FeCl_3$,the iron source, reduces with ethylene glycol, as both solvent and the reducing agent, in the presence of trisodium citrate and sodium acetate as electrostatic and alkali sources, respectively. Then, to avoid the agglomeration of magnetic nanoparticles and the oxidation in air, the particles were coated with silica shell through a sol–gel process. Also, SiO_2 shell is needed to attain the desired yolk–shell structure. Subsequently, the branched PEI was used to modify the surface of Fe_3O_4@-SiO_2. bPEI possesses nitrogen containing tridentate ligands which results in effectively coordination to Cu(I).[45] In continuation, to reduce the density of positive charge of bPEI and consequently to modify the interation of bPEI with Cu(I), ethylated bPEI was synthesized through nucleophilic attack of amine groups of bPEI to ethyle iodide in the presence of potassium carbonate as a base. Then, the perferential etching of middle SiO_2 layer was accomplished using NaOH to obtain the yolk–shell structure with magnetic core inside the hollow ethylated-bPEI shell. Finally, Cu(I) was introduced to the YS Fe_3O_4@Et-bPEI to achieve the desired catalyst YS Fe_3O_4@Et-bPEI@Cu(I). Negative charge density of nitrogen groups in the bPEI causes the interaction with positively charged Cu(I).

Table I. The Polymerization of Styrene with YS Fe_3O_4@Et-bPEI@Cu(I) as the Supported Catalyst and 2-Bromoisobutyryl Bromide as the Initiator[a]

Entry	Time (h)	Conv.[b] (%)	M_n[c]	M_n[d]	PDI[e]
1	1.5	21	2812.3	2101.82	1.78
2	2.5	28	2894.3	2361.8	1.80
3	4.5	35	2980.8	2465.82	1.77

[a] Polymerization conditions: 100/0.15/1 [St]/[Cu]/BIBB in toluene at 90°C.
[b] Conversions determined by gas chromatography.
[c] The number average molecular weight (M_n) determined by GPC calibrated against PS standards.
[d] Calculated by ^{1}H NMR.
[e] Molecular weight distribution (M_w/M_n).

Analysis

FT-IR Analysis. FT-IR spectra of Fe_3O_4 magnetic particles, Fe_3O_4@SiO_2, Fe_3O_4@SiO_2@bPEI, and YS Fe_3O_4@Et-bPEI were shown in Figure 1(A–D), respectively. The FT-IR spectrum of Fe_3O_4 magnetic particles indicates two bands located at 1629 and 1412 cm^{-1} ascribed to the carboxylate group of citrate. The peaks observed at 593 and 3413 cm^{-1} are related to Fe—O and O—H stretching vibrations, respectively. In Figure 1(B), the absorption peaks at 1089 and 801 cm^{-1} are attributed to the symmetrical and asymmetrical stretching vibrations of Si—O—Si, respectively. The FT-IR spectrum of Fe_3O_4@SiO_2@b-PEI demonstrates a broad peak at 3440 cm^{-1} due to the N—H stretching vibration, while the bands located at 2933 and 2856 cm^{-1} are related to CH_2 stretching vibrations of the bPEI chain. C—N stretching vibration is typically appeared at around 1000–1200 cm^{-1}, however this peak cannot be seen due to its coverage by the intense Si—O—Si peak in the same range [Figure 1(C)]. In FT-IR spectrum of YS Fe_3O_4@Et-bPEI, the absorption peak of Si—O—Si has been removed, showing the completely etching of the intermediate SiO_2 layer by NaOH solution, and consequently the vibrations of C—N groups are observed.

XRD Analysis. Figure 2 shows the XRD patterns for Fe_3O_4 (A), Fe_3O_4@SiO_2@bPEI (B), YS Fe_3O_4@Et-bPEI (C), and YS Fe_3O_4@Et-bPEI@Cu(I) (D). In Figure 2(A), six characteristic diffraction peaks appeared at $2\theta = 29.85°$, 35.43°, 43.07°, 56.96°, 62.67°, and 74.21° are related to (220), (311), (400), (511), (440), (622) Bragg diffractions of face centered cubic structured Fe_3O_4 magnetic particles (JCPDS no. 19–629). The XRD pattern of Fe_3O_4@SiO_2@bPEI shows a broad diffraction peak around $2\theta = 23.35°$ related to the amorphous silica shell, besides the diffraction peaks of Fe_3O_4. The peak at $2\theta = 23.35°$ was disappeared in Figure 2(C) due to the removal of middle silica layer. Figure 2(D) illustrates three additional peaks at $2\theta = 37°$, 44°, and 62° attributed to (111), (200), (220) diffractions of Cu (I) in the synthesized YS Fe_3O_4@Et-bPEI@Cu(I).

TGA Analysis. The relative amount of Et-bPEI grafted onto the surface of Fe_3O_4@SiO_2 was estimated by TGA measurements. Figure 3(A,B) shows the TGA curves of Fe_3O_4@SiO_2 and Fe_3O_4@SiO_2@Et-bPEI. The thermogram of Fe_3O_4@SiO_2@Et-bPEI displays two steps of degradation, the first step at below 230°C is related to the elimination of moisture. The weight loss at 230°C–660°C is attributed to Et-bPEI decomposition. Based on the percentage of the remaining mass of Fe_3O_4@SiO_2@Et-bPEI and comparing with Fe_3O_4@SiO_2, we can estimate the

Table II. The Effect of Temperature on the Polymerization of Styrene with YS Fe_3O_4@Et-bPEI@Cu(I) as the Supported Catalyst and 2-Bromoisobutyryl Bromide as the Initiator[a]

Entry	Time (h)	Conv.[b] (%) (70°C)	M_n[c] (70°C)	M_n[d] (70°C)	PDI[e] (70°C)	Conv.[b] (%) (80°C)	M_n[c] (80°C)	M_n[d] (80°C)	PDI[e] (80°C)
1	1.5	13	2597.62	1940.62	1.78	12	2683.51	2005.31	1.73
2	2.5	18	2806.97	2290.08	1.76	20	2819.22	2300.02	1.78
3	4.5	20	2816.45	2318.08	1.79	26	2871.19	2375.34	1.78

[a] Polymerization conditions: 100/0.15/1 [St]/[Cu]/BIBB in toluene.
[b] Conversions determined by gas chromatography.
[c] The number average molecular weight (M_n) determined by GPC calibrated against PS standards.
[d] Calculated by ^{1}H NMR.
[e] Molecular weight distribution (M_w/M_n).

weight fraction of Et-bPEI to be 6.6% by excluding the weight losses related to the water elimination.

UV–Visible Analysis. UV–vis spectra of Fe_3O_4@SiO_2@Et-bPEI, YS Fe_3O_4@Et-bPEI, and YS Fe_3O_4@Et-bPEI@Cu(I) in acetonitrile at 25°C were given in Figure 4(A–C), respectively. Figure 4A shows a broad peak at about 390 nm which indicates the existence of the core–shell Fe_3O_4@SiO_2. We also measured the UV–vis spectrum of YS Fe_3O_4@Et-bPEI spheres, which showed no significant peak [Figure 4(B)]. A broad absorption band at 375 nm and the absence of the peak around 660 nm, attributed to Cu(II), in the UV–vis spectrum of YS Fe_3O_4@Et-bPEI@Cu(I) confirmed the existence of Cu(I).

SEM and TEM Analyses. The uniform spherical morphology of YS Fe_3O_4@Et-bPEI@Cu(I) is also verified by the SEM images shown in Figure 5(A,B). The thickness of nanoparticles can be tuned in the range of 80–95 nm. The TEM observation shows the yolk/shell structured nanospheres synthesized using Fe_3O_4 spheres as the core and ethylated-bPEI as the shell. Two distinct components, the black cores of Fe_3O_4, the gray shells of Et-bPEI can be observed. It is apparent that yolk/shell spheres are obtained [Figure 5(C,D)].

VSM Analysis. Figure 6(A,B) shows the magnetization curves of pure Fe_3O_4, and YS Fe_3O_4@Et-bPEI@Cu(I) nanoparticles, respectively, determined by VSM at room temperature. The saturation magnetizations were found to be 70.1 and 42.1 emu/g, for Fe_3O_4 and the as-prepared catalyst, respectively. Moreover, the results indicated that these magnetic nanoparticles are superparamagnetic with zero values for both remanence and coercivity in the hysteresis loop (Figure 6).

Catalytic Activity of YS Fe_3O_4@Et-bPEI@Cu(I) for ATRP Reaction of Styrene

As mentioned before, ATRP has been a very important industrial process due to the preparation of polymers with predetermined molecular weights and complex architectures from a large variety of monomers.[21] In this work, the catalytic activity of Cu(I) stabilized on YS Fe_3O_4@Et-bPEI was investigated for the ATRP reaction of styrene in the presence of 2-bromoisobutyryl bromide as the initiator in toluene as a model reaction. It should be notable that very low amounts of the catalyst were used which is very important to improve the livingness of ATRP.[46] First, the model reaction was performed for 1.5, 2.5, and 4.5 h with 0.15 mol % Cu, and 0.0395 mmol 2-bromoisobutyryl bromide at 90°C which 21%, 28%, and 35% conversions were obtained (Table I).

When YS Fe_3O_4@Et-bPEI@Cu(I) was used as the supported catalyst in the copper-based ATRP reactions of styrene, the molecular weights that measured by GPC were near to the predicted molecular weights (Table I).

To investigate the effect of temperature, the ATRP reaction of styrene was also carried out at 70°C, and 80°C and the conversions were measured by GC. Under the same conditions, with decreasing the temperature from 90°C to 70°C, the molecular

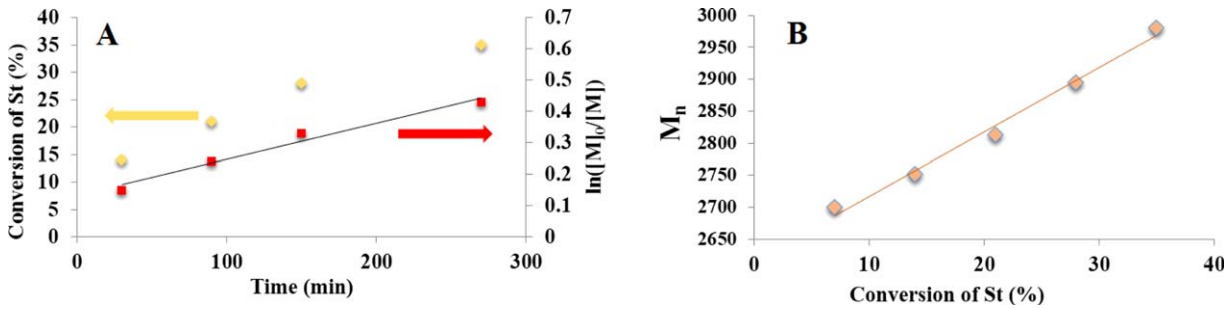

Figure 7. Dependence of monomer conversion and $\ln([M]_0/[M])$ on time (**A**), and dependence of molecular weight on conversion (**B**) for ATRP reaction of styrene with YS Fe_3O_4@Et-bPEI@Cu(I) as a supported catalyst. [Color figure can be viewed in the online issue, which is available at wileyonlinelibrary.com.]

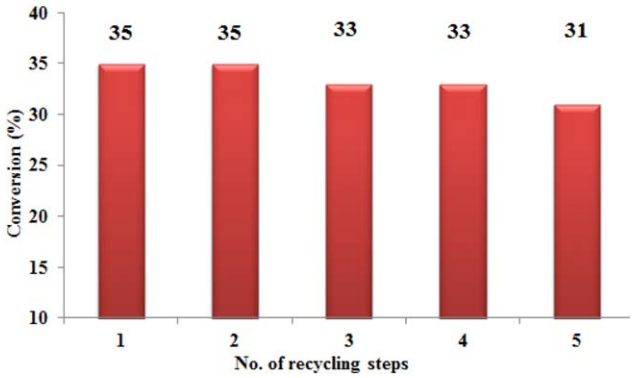

Figure 8. Effect of recycling on the catalytic efficiency of YS Fe_3O_4@Et-bPEI@Cu(I). [Color figure can be viewed in the online issue, which is available at wileyonlinelibrary.com.]

weights decreased, but the molecular weight distributions did not change significantly (Table II).

A linear dependence of $\ln([M]_0/[M])$ versus time [Figure 7(A)] indicated that the polymerization reactions are first order with respect to the monomer concentration and the concentration of propagating species during the polymerization are constant. The linearly increasing M_n with monomer conversion [Figure 7(B)], and the fairly narrow molecular weight distributions also verified the controlled radical polymerization behavior.

Residual Copper

Atomic absorption spectroscopy was applied to determine the residual copper content in the polymer product after the reaction. According to the AAS, 3.8 ppm of Cu remained in the final polystyrene (PS) product after the magnetic extraction and the first precipitation from methanol. The copper concentration was reduced to 1.1 ppm after the second precipitation step which is considerably better than the other reported value with a heterogeneous catalyst system.[47]

Recycling YS Fe_3O_4@Et-bPEI@Cu(I)

To investigate the recyclability of the as-prepared catalyst, we tested the ATRP reaction of styrene as a model reaction after 4.5 h for five cycles. The results are presented in Figure 8, which indicated that the conversions after every run did not change considerably, demonstrating the high stability of the catalyst. The polymers obtained after each run still possess relatively low polydispersity similar to the product of the first run. Notably, the magnetic extraction eliminates the need for filtration or centrifugation steps.

CONCLUSIONS

In this work, copper(I) stabilized on the yolk–shell Fe_3O_4@ethylated-bPEI was successfully synthesized and characterized. We chose the yolk–shell structure because it has high surface area, low density, and larger vacant space compared with the corresponding core–shell structure. Using ethylated-branched PEI with tridentate nitrogen containing ligands was led to stabilize copper ions effectively which is a critical point in ATRP reactions. The polymerization of styrene as a model reaction was studied at different temperatures using YS Fe_3O_4@Et-bPEI@Cu(I) in toluene and with 2-bromoisobutyryl bromide as a initiator. The polymerization reactions were successfully performed achieving high control over molecular weight and small molecular weight distribution. The catalyst was magnetically recoverable and was used for five cycles without significant loss in activity. The very low amount of the residual copper in the polymer product is one of the most important advantages of this catalyst. Moreover, the preliminary tests of this supported catalyst for the ATRP of acrylate monomers are still in progress.

ACKNOWLEDGMENTS

We are grateful to Shahid Beheshti University Research Council for partial financial support of this work.

REFERENCES

1. Kato, M.; Kamigaito, M.; Sawamoto, M.; Higashimura, T. *Macromolecules* **1995**, *28*, 1721.
2. Kamigaito, M.; Ando, T.; Sawamoto, M. *Chem. Rev.* **2001**, *101*, 3689.
3. Matyjaszewski, K. *Macromolecules* **2012**, *45*, 4015.
4. Poli, R. *Angew. Chem. Int. Ed.* **2006**, *45*, 5058.
5. Peng, C.-H.; Kong, J.; Seeliger, F.; Matyjaszewski, K. *Macromolecules* **2011**, *44*, 7546.
6. di Lena, F.; Matyjaszewski, K. *Prog. Polym. Sci.* **2010**, *35*, 959.
7. Braunecker, W. A.; Itami, Y.; Matyjaszewski, K. *Macromolecules* **2005**, *38*, 9402.
8. Debuigne, A.; Caille, J. R.; Jérôme, R. *Angew. Chem. Int. Ed.* **2005**, *44*, 1104.
9. Li, P.; Qiu, K.-Y. *Polymer* **2002**, *43*, 5873.
10. Kabachii, Y. A.; Kochev, S. Y.; Bronstein, L. M.; Blagodatskikh, I. B.; Valetsky, P. M. *Polym. Bull.* **2003**, *50*, 271.
11. Patten, T. E.; Matyjaszewski, K. *Acc. Chem. Res.* **1999**, *32*, 895.
12. Tsarevsky, N. V.; Matyjaszewski, K. *Chem. Rev.* **2007**, *107*, 2270.
13. Coullerez, G.; Carlmark, A.; Malmström, E.; Jonsson, M. *J. Phys. Chem. A* **2004**, *108*, 7129.
14. Braunecker, W. A.; Matyjaszewski, K. *Prog. Polym. Sci.* **2007**, *32*, 93.
15. Shen, Y.; Tang, H.; Ding, S. *Prog. Polym. Sci.* **2004**, *29*, 1053.
16. Tsarevsky, N. V.; Matyjaszewski, K. *J. Polym. Sci., Part A: Polym. Chem.* **2006**, *44*, 5098.
17. Kubisa, P. *Prog. Polym. Sci.* **2004**, *29*, 3.
18. Pyun, J.; Matyjaszewski, K.; Kowalewski, T.; Savin, D.; Patterson, G.; Kickelbick, G.; Huesing, N. *J. Am. Chem. Soc.* **2001**, *123*, 9445.
19. Fournier, D.; Pascual, S.; Montembault, V.; Fontaine, L. *J. Polym. Sci., Part A: Polym. Chem.* **2006**, *44*, 5316.
20. Tang, W.; Matyjaszewski, K. *Macromolecules* **2006**, *39*, 4953.
21. Matyjaszewski, K.; Xia, J. *Chem. Rev.* **2001**, *101*, 2921.
22. Choosakoonkriang, S.; Lobo, B. A.; Koe, G. S.; Koe, J. G.; Middaugh, C. R. *J. Pharm. Sci.* **2003**, *92*, 1710.

23. Zorvaryan, A.; Inceoglu, S.; Acar, M. H. *Polymer* **2011**, *52*, 617.
24. Godbey, W.; Wu, K. K.; Mikos, A. G. *Biomaterials* **2001**, *22*, 471.
25. Corti, M.; Lascialfari, A.; Marinone, M.; Masotti, A.; Micotti, E.; Orsini, F.; Ortaggi, G.; Poletti, G.; Innocenti, C.; Sangregorio, C. *J. Magn. Magn. Mater.* **2008**, *320*, e316.
26. Liu, J.; Qiao, S. Z.; Chen, J. S.; Lou, X. W. D.; Xing, X.; Lu, G. Q. M. *Chem. Commun.* **2011**, *47*, 12578.
27. Priebe, M.; Fromm, K. M. *Chem. Eur. J.* **2015**, *21*, 3854.
28. Zhang, L.; Wang, T.; Yang, L.; Liu, C.; Wang, C.; Liu, H.; Wang, Y. A.; Su, Z. *Chem. Eur. J.* **2012**, *18*, 12512.
29. Liu, N.; Wu, H.; McDowell, M. T.; Yao, Y.; Wang, C.; Cui, Y. *Nano Lett.* **2012**, *12*, 3315.
30. Zhang, L.; Wang, T.; Liu, P. *Chem. Eng. J.* **2012**, *187*, 372.
31. Galeano, C.; Baldizzone, C.; Bongard, H.; Spliethoff, B.; Weidenthaler, C.; Meier, J. C.; Mayrhofer, K. J.; Schüth, F. *Adv. Funct. Mater.* **2014**, *24*, 220.
32. Yue, Q.; Zhang, Y.; Wang, C.; Wang, X.; Sun, Z.; Hou, X.-F.; Zhao, D.; Deng, Y. *J. Mater. Chem. A* **2015**, *3*, 5730.
33. Yao, Y.; Zhang, X.; Peng, J.; Yang, Q. *Chem. Commun.* **2015**, *51*, 3750.
34. Yin, Y.; Rioux, R. M.; Erdonmez, C. K.; Hughes, S.; Somorjai, G. A.; Alivisatos, A. P. *Science* **2004**, *304*, 711.
35. Ma, W.-F.; Zhang, C.; Zhang, Y.-T.; Yu, M.; Guo, J.; Zhang, Y.; Lu, H.-J.; Wang, C.-C. *Langmuir* **2014**, *30*, 6602.
36. Zeng, T.; Zhang, X.; Wang, S.; Ma, Y.; Niu, H.; Cai, Y. *Chem. Eur. J.* **2014**, *20*, 6474.
37. Nabid, M. R.; Bide, Y.; Tabatabaei Rezaei, S. J. *Appl. Catal. A* **2011**, *406*, 124.
38. Nabid, M. R.; Bide, Y.; Niknezhad, M. *ChemCatChem* **2014**, *6*, 538.
39. Nabid, M. R.; Bide, Y. *Appl. Catal. A* **2014**, *469*, 183.
40. Nabid, M.; Bide, Y.; Aghaghafari, E.; Rezaei, S. *Catal. Lett.* **2014**, *144*, 355.
41. Nabid, M. R.; Bide, Y.; Abuali, M. *RSC Adv.* **2014**, *4*, 35844.
42. Nabid, M. R.; Bide, Y.; Habibi, Z. *RSC Adv.* **2015**, *5*, 2258.
43. Nabid, M. R.; Bide, Y.; Ghalavand, N.; Niknezhad, M. *Appl. Organomet. Chem.* **2014**, *28*, 389.
44. Liu, J.; Sun, Z.; Deng, Y.; Zou, Y.; Li, C.; Guo, X.; Xiong, L.; Gao, Y.; Li, F.; Zhao, D. *Angew. Chem. Int. Ed.* **2009**, *48*, 5875.
45. Matyjaszewski, K.; Göbelt, B.; Paik, H.-J.; Horwitz, C. P. *Macromolecules* **2001**, *34*, 430.
46. Wang, Y.; Soerensen, N.; Zhong, M.; Schroeder, H.; Buback, M.; Matyjaszewski, K. *Macromolecules* **2013**, *46*, 683.
47. Kickelbick, G.; Paik, H.-j.; Matyjaszewski, K. *Macromolecules* **1999**, *32*, 2941.